

# Error and stability analysis of an anisotropic phase-field model for binary-fluid mixtures in the presence of magnetic-field

A. Rasheed\*, A. Belmiloudi†

## Abstract

In this article, we study the error and stability of the proposed numerical scheme in order to solve a two dimensional anisotropic phase-field model with convection and externally applied magnetic field in an isothermal solidification of binary alloys. The proposed numerical scheme is based on mixed finite element method satisfying the CFL condition. A particular application with real physical parameters of Nickel-Copper(Ni-Cu) is considered in order to validate the numerical scheme employed. The results of stability and error analysis substantiates complete accordance with the postulated theoretical error estimates which demonstrates the efficiency of the presented method.

**keyword** Phase field methods; Stability and error analysis; binary alloys; magnetic-field.

## 1 Introduction

The quality of the final solidified metal is dependent on the dendrite structure evolution during the process of solidification of metals. In order to ameliorate the quality of the solidified materials, it is important to understand and render control over dendritic structure formation during the process of solidification of alloys. During the past decade, the scientists have investigated a great deal of experimental and theoretical studies to explore the microstructure of dendrites during the process of solidification of alloys. Phase field method has been widely used by researchers in order to simulate and study the structure and formation of dendrites (see for instance [1, 2, 3, 6, 10, 15, 16, 17, 27, 29, 30, 31]) and the references therein. Unfortunately, the presented models donot render control on dendritic evolution and micro-segregation. Moreover, some experimental observations show that the control on dendrite growth can be achieved in the during the solidification process by applying electric and magnetic fields externally, see for example [14, 24] and the references therein. For similar other applications wherin authors have discussed the effect of magnetic field on the metals and alloys, refer to the studies, e.g., for the semi-conductor flow in the melt crystal evolution, [7], for the MHD flows [12], [11], [32], [9] and for the processes of dendritic solidification, [23], [24], [25] and the references therein.

In view of aforementioned facts, Rasheed and Belmiloudi in [20] (see also [18, 19, 22]) has presented a phase-field model which incorporates melt flow and magnetic field. Initially, the model of Warren-Boettinger [31] is considered and then, among other, Navier Stokes equations, the phase-field and solute equations with a magnetic field applied externally on the domain. The newly developed phase-field model consists three systems, the magnetohydrodynamic system which describes the melt convection by using incompressible Navier-Stokes equations together with the Lorentz force and boussinesq approximations, the phase-field system which represents the phase change and the concentration system describing the concentration change in dendrites during solidification process. The phase field and concentration equations are of convection diffusion type systems. We refer the reader to [20] for more detailed description of the model.

The existence and uniqueness of the solutions of the derived model is presented in the article [20]. In order to perform realistic physical simulations it is indispensable to develop a stable and convergent

---

\*Department of Mathematics, Lahore University of Management Sciences, Opposite Sector U, DHA,Lahore Cantt 54792, Pakistan, amer.rasheed@lums.edu.pk,

†Mathematics Research Institute of Rennes (IRMAR), European University of Brittany, INSA, 20 Av. Buttes de Coesmes, CS70839, 35708 Rennes Cedex7, France, aziz.belmiloudi@math.cnrs.fr

numerical scheme. This article is devoted to present a numerical approximation scheme using mixed finite-elements and numerical stability and error analysis for Rasheed and Belmiloudi model [?] for the anisotropic case. Some numerical results in the isotropic case are presented in the article [21].

The paper has been organized as follows. In section 2 we recall the mathematical model briefly and its weak formulation in section 3. Section 4 describes the discrete variational formulation, in the context of a mixed finite element method. The numerical stability and error analysis are presented and validated by numerical experiments in section 5.

## 2 Mathematical formulation

Initially a region  $\Omega$  is assumed to be occupied by a binary alloy containing two pure elements, the solute B (e.g., Cu) and the solvent A (e.g., Ni), which is electrically conducting incompressible fluid. To construct a numerical scheme and study its numerical stability and error, we recall the model for dendritic solidification given by [20]. Let  $\mathbf{u}$ ,  $p$ ,  $\psi$ ,  $c$  and  $\mathbf{B}$  represent the velocity vector, pressure, phase-field variable, relative concentration and externally magnetic field respectively. We have the following system

$$\begin{cases} \rho_0(\partial_t \mathbf{u} + (\mathbf{u} \cdot \nabla) \mathbf{u}) = -\nabla p + \mu \Delta \mathbf{u} + \mathcal{A}_1(\psi, c) + b(\psi)((\mathbf{u} \times \mathbf{B}) \times \mathbf{B}) & \text{on } \mathcal{Q}, \\ \operatorname{div} \mathbf{u} = 0 & \text{on } \mathcal{Q}, \\ \partial_t \psi + (\mathbf{u} \cdot \nabla) \psi = \operatorname{div}(\mathcal{A}_g(\nabla \psi) \nabla \psi) - \mathcal{A}_2(\psi, c) & \text{on } \mathcal{Q}, \\ \partial_t c + (\mathbf{u} \cdot \nabla) c = \operatorname{div}(D(\psi) \nabla c + \mathcal{A}_3(\psi, c) \nabla \psi) & \text{on } \mathcal{Q}, \\ \text{subject to the initial conditions} & \\ (\mathbf{u}, \psi, c)(t=0) = (\mathbf{u}_0, \psi_0, c_0) & \text{on } \Omega, \\ \text{and the boundary conditions} & \\ \mathbf{u} = 0, \quad \mathcal{A}_g(\nabla \psi) \nabla \psi \cdot \mathbf{n} = 0, \quad (D(\psi) \nabla c + \mathcal{A}_3(\psi, c) \nabla \psi) \cdot \mathbf{n} = 0 & \text{on } \Sigma, \end{cases} \quad (2.1)$$

where  $\Omega \subset \mathbb{R}^2$  is a Lipschitz and sufficiently smooth open solidification domain with polygonal boundary  $\partial\Omega$ ,  $T$  is the final time of the solidification process,  $\mathcal{Q} = \Omega \times (0, T)$ ,  $\Sigma = \partial\Omega \times (0, T)$ ,  $\rho_0 = \frac{\rho_0^{(A)} + \rho_0^{(B)}}{2}$  and  $\mu = \frac{\mu^{(A)} + \mu^{(B)}}{2}$  are the average density and viscosity,  $D(\psi)$  is the diffusion coefficient and  $\mathbf{n}$  is the unit outward normal to  $\partial\Omega$ . The anisotropy matrix  $\mathcal{A}_g$  is defined by

$$\mathcal{A}_g(\nabla \psi) = M_\psi \begin{pmatrix} \eta_\gamma^2(\theta) & -\eta_\gamma(\theta) \eta'_\gamma(\theta) \\ \eta_\gamma(\theta) \eta'_\gamma(\theta) & \eta_\gamma^2(\theta) \end{pmatrix}$$

where  $M_\psi > 0$  and  $\eta_\gamma$  is the anisotropy function defined as [31]

$$\eta_\gamma = \epsilon_0(1 + \gamma \cos(k\theta)), \quad (2.2)$$

$\gamma \geq 0$  is the anisotropic amplitude, the integer  $k > 1$  corresponds to the number of branching directions,  $\epsilon_0$  is a constant and  $\theta$  (the angle between the  $x$ -axis and  $\nabla \psi$ )

$$\theta = \arctan\left(\frac{\psi_y}{\psi_x}\right), \quad (2.3)$$

where  $x$  and  $y$  are subscripts used to represent the partial derivatives with respect to spatial coordinates, that is  $\psi_x = \partial\psi/\partial x$  and  $\psi_y = \partial\psi/\partial y$ . For low to moderate accuracy,  $\gamma > 0$  is selected so that the condition  $\eta_\gamma(\theta) + \frac{d^2 \eta_\gamma}{d\theta^2}(\theta) > 0$  is valid for all  $\theta$ . For  $k = 4$  (fourfold anisotropy) which is a case of physical appearance, the previous condition is valid if  $\gamma < \frac{1}{15} \approx 0,6667$ . The operators  $\mathcal{A}_1$ ,  $\mathcal{A}_2$  and  $\mathcal{A}_3$  are defined by

$$\begin{aligned} \mathcal{A}_1(\psi, c) &= \beta_c a_1(\psi) c \mathbf{G} + \zeta \mathbf{f}(\psi), \quad \mathcal{A}_2(\psi, c) = M_\psi \left( \frac{\lambda_1(c)}{\delta^2} g'(\psi) + \frac{\lambda_2(c)}{\delta} \bar{p}'(\psi) \right), \\ \mathcal{A}_3(\psi, c) &= \alpha_0 D(\psi) c (1 - c) \left( \frac{\lambda'_1(c)}{\delta} g'(\psi) - \lambda'_2(c) \bar{p}'(\psi) \right), \end{aligned} \quad (2.4)$$

For a detailed description and derivation of the mathematical model, the reader is referred to [20].

### 3 Weak formulation

The inner product and norm in  $L^2(\Omega)$  are defined respectively by  $(\cdot, \cdot)$  and  $|\cdot|$  and

$$\begin{aligned} \mathcal{W} &= (H_0^1(\Omega))^2 = \left\{ \mathbf{v} \in (H^1(\Omega))^2 \mid \mathbf{v} = 0 \text{ on } \partial\Omega \right\}, & \mathcal{W}_d &= \{ \mathbf{v} \in \mathcal{W} \mid \operatorname{div}(\mathbf{v}) = 0 \}, \\ \mathcal{M} &= H^1(\Omega), & \mathcal{H} &= \left\{ q \in L^2(\Omega) \mid \int_{\Omega} q d\mathbf{x} = 0 \right\}, \end{aligned} \quad (3.1)$$

where  $\mathcal{W}$  is equipped with the norm  $\|\nabla \cdot\|$ . The scalar product and norm in  $\mathcal{H}$  are denoted by the usual  $L^2(\Omega)$  inner product and its norm  $(\cdot, \cdot)$  and  $|\cdot|$ , respectively.

**Remark 3.1** : *In order to assure that the pressure is unique, we impose the condition  $\int_{\Omega} q d\mathbf{x} = 0$  on the pressure which is defined within a class of equivalence, regardless of a time-dependent function. We may impose also other conditions on the pressure, in accordance on its regularity, e.g., the pressure is constant on part of the boundary, etc.*

The bilinear and trilinear forms are defined as follows (for all  $(\mathbf{u}, \mathbf{v}, \mathbf{w}) \in (\mathcal{W})^3$ ,  $p \in \mathcal{H}$ ,  $(c, z) \in (\mathcal{M})^2$  and  $(\phi, \psi) \in (\mathcal{M})^2$ ):

$$\begin{aligned} a_u(\mathbf{u}, \mathbf{v}) &= \mu \int_{\Omega} \nabla \mathbf{u} \cdot \nabla \mathbf{v} d\mathbf{x}, & c_p(\mathbf{u}, p) &= -(\operatorname{div}(\mathbf{u}), p), & b_u(\mathbf{u}, \mathbf{v}, \mathbf{w}) &= \rho_0 \sum_{i,j=1}^2 \int_{\Omega} u_i (\partial_i v_j) w_j d\mathbf{x}, \\ b_c(\mathbf{u}, c, z) &= \sum_{i=1}^2 \int_{\Omega} u_i (\partial_i c) z d\mathbf{x}, & b_{\psi}(\mathbf{u}, \psi, \phi) &= \sum_{i=1}^2 \int_{\Omega} u_i (\partial_i \psi) \phi d\mathbf{x}. \end{aligned}$$

Moreover, if  $\operatorname{div}(\mathbf{u}) = 0$ , the trilinear forms satisfy the classical relations given in the following Lemma (see e.g. [5, 28]):

**Lemma 3.1** *The trilinear forms  $b_u, b_{\psi}, b_c$  have the following properties*

(i) *For all  $\mathbf{u} \in \mathcal{W}_d$ ,  $\mathbf{v} \in \mathcal{W}$  and  $\psi, c \in \mathcal{M}$*

$$b_u(\mathbf{u}, \mathbf{v}, \mathbf{v}) = 0, \quad b_{\psi}(\mathbf{u}, \psi, \psi) = 0, \quad b_c(\mathbf{u}, c, c) = 0.$$

(ii) *For all  $\mathbf{u} \in \mathcal{W}_d$ ,  $\mathbf{v}, \mathbf{w} \in \mathcal{W}$  and  $\psi, \phi, c, z \in \mathcal{M}$*

$$b_u(\mathbf{u}, \mathbf{v}, \mathbf{w}) = -b_u(\mathbf{u}, \mathbf{w}, \mathbf{v}), \quad b_{\psi}(\mathbf{u}, \psi, \phi) = -b_{\psi}(\mathbf{u}, \phi, \psi), \quad b_c(\mathbf{u}, c, z) = -b_c(\mathbf{u}, z, c).$$

In order to obtain the weak formulations of the underlying model we multiply the first and second equations of (2.1) by  $\mathbf{v} \in \mathcal{W}$ , third equation of (2.1) by  $\phi \in \mathcal{M}$  and last equation of (2.1) by  $z \in \mathcal{M}$ . Further we integrate the results over  $\Omega$  and then using Green's formulas and boundary conditions, we obtain the following weak formulation of the problem (2.1) (wherein we added an artificial source term  $\mathbf{F}_u, F_{\psi}$  and  $F_c$  in each equation of the model for fabricating exact solutions to perform the convergence and stability of the numerical scheme): Find  $(\mathbf{u}, p, \psi, c) \in \mathcal{W} \times \mathcal{H} \times \mathcal{M} \times \mathcal{M}$  such that  $\forall (\mathbf{v}, q, \varphi, z) \in \mathcal{W} \times \mathcal{H} \times \mathcal{M} \times \mathcal{M}$

$$\left\{ \begin{array}{l} \rho_0 (\partial_t \mathbf{u}, \mathbf{v}) + a_u(\mathbf{u}, \mathbf{v}) + b_u(\mathbf{u}, \mathbf{u}, \mathbf{v}) + c_p(\mathbf{v}, p) - (\mathcal{A}_1(\psi, c), \mathbf{v}) \\ \quad - (b(\psi)((\mathbf{u} \times \mathbf{B}) \times \mathbf{B}), \mathbf{v}) = (\mathbf{F}_u, \mathbf{v}), \\ -c_p(\mathbf{u}, q) = 0, \\ (\partial_t \psi, \varphi) + b_{\psi}(\mathbf{u}, \psi, \varphi) + (\mathcal{A}_g(\nabla \psi) \nabla \psi, \nabla \varphi) + (\mathcal{A}_2(\psi, c), \varphi) = (F_{\psi}, \varphi), \\ (\partial_t c, z) + b_c(\mathbf{u}, c, z) + (D(\psi) \nabla c, \nabla z) + (\mathcal{A}_3(\psi, c) \nabla \psi, \nabla z) = (F_c, z), \\ (\mathbf{u}, \psi, c)(t=0) = (\mathbf{u}_0, \psi_0, c_0). \end{array} \right. \quad (3.2)$$

## 4 Discrete weak formulation and finite element discretization

Let  $\mathcal{T}_h$  be a family of triangulations which discretize the domain  $\bar{\Omega}$  with maximum mesh spacing parameter  $0 < h = \max_{\mathcal{U} \in \mathcal{T}_h} \text{diam}(\Omega) < h_0 < 1$ . To develop the Galerkin approximation of (3.2), we consider the  $\mathbb{P}_l$ ,  $\mathbb{P}_{l-1}$  and  $\mathbb{P}_l$  finite element subspaces  $\mathcal{W}_h$ ,  $\mathcal{H}_h$  and  $\mathcal{M}_h$  of  $\mathcal{W}$ ,  $\mathcal{H}$  and  $\mathcal{M}$  respectively over the partition  $\mathcal{T}_h$ , where the polynomials  $\mathbb{P}_l$  is the space of polynomials of degree at most  $l$ . Furthermore, in order to derive theoretical error estimates of the PDEs like 2.1, we impose the following assumptions (see [4, 26])

(C1)  $\exists c_1 > 0$ , such that  $\forall \mathbf{X} = (\mathbf{u}, \psi, c) \in (H^{r+1}(\Omega))^4 \cap (\mathcal{W} \times \mathcal{M}^2)$  and  $\forall r \in [1, l]$

$$\inf_{\mathbf{X}_h \in \mathcal{W}_h \times \mathcal{M}_h^2} \|\mathbf{X} - \mathbf{X}_h\| \leq c_1 h^r \|\mathbf{X}\|_{H^{r+1}(\Omega)}.$$

(C2)  $\exists c_2 > 0$ , such that  $\forall q \in H^r(\Omega) \cap \mathcal{H}$  and  $\forall r \in [1, l]$

$$\inf_{q_h \in \mathcal{H}_h} \|q - q_h\| \leq c_2 h^r \|q\|_{H^r(\Omega)}.$$

(C3)  $\exists c_3 > 0$  such that (Inf-Sup condition)

$$\inf_{q_h \in \mathcal{H}_h} \sup_{\mathbf{v}_h \in \mathcal{W}_h} \frac{c_p(\mathbf{v}_h, q_h)}{\|\mathbf{v}_h\| \|q_h\|} \geq c_3.$$

(C4) Let  $\mathbf{X}_0 = (\mathbf{u}_0, \psi_0, c_0) \in (H^{r+1}(\Omega))^4$  with  $r \in [1, l]$ , then

$$h \|\mathbf{X}_0 - \mathbf{X}_{0h}\| + |\mathbf{X}_0 - \mathbf{X}_{0h}| \leq c_4 h^{r+1},$$

where  $\mathbf{X}_{0h} = (\mathbf{u}_{0h}, \psi_{0h}, c_{0h}) \in \mathcal{W}_h \times \mathcal{M}_h^2$  is the approximation of  $\mathbf{X}_0$ .

(C5) For all integers  $\mathbf{m}, \mathbf{p}, \mathbf{q}$  and  $\mathbf{k}$  with  $0 < \mathbf{p}, \mathbf{q} \leq \infty$  and  $\forall K \in \mathcal{T}_h$ , we have

$$\begin{aligned} \|\mathbf{X}_h\|_{W^{\mathbf{m}, \mathbf{q}}(K)} &\leq c_4 h^{n/q - n/\mathbf{p} + \mathbf{k} - \mathbf{m}} \|\mathbf{X}_h\|_{W^{\mathbf{k}, \mathbf{p}}(K)}, \quad \forall \mathbf{X}_h \in \mathcal{W}_h \times \mathcal{M}_h^2, \\ \|\mathbf{X}_h\|_{W^{\mathbf{m}, \mathbf{q}}(\Omega)} &\leq c_4 h^{n/q - n/\mathbf{p} + \mathbf{k} - \mathbf{m}} \|\mathbf{X}_h\|_{W^{\mathbf{k}, \mathbf{p}}(\Omega)}, \quad \forall \mathbf{X}_h \in \mathcal{W}_h \times \mathcal{M}_h^2. \end{aligned}$$

The space and time discretization of the problem (3.2) i.e. the discrete weak formulation of the problem (2.1) can now be easily defined. We shall describe in detail the numerical scheme and present the space discretization and the general form of the differential-algebraic systems for (3.2). Further we present the time discretization of the problem briefly. The discrete weak formulation is presented as follows: Find  $(\mathbf{u}_h, p_h, \psi_h, c_h) \in \mathcal{W}_h \times \mathcal{H}_h \times \mathcal{M}_h \times \mathcal{M}_h$  such that  $\forall (\mathbf{v}_h, q_h, \varphi_h, z_h) \in \mathcal{W}_h \times \mathcal{H}_h \times \mathcal{M}_h \times \mathcal{M}_h$

$$\left\{ \begin{array}{l} \rho_0 (\partial_t \mathbf{u}_h, \mathbf{v}_h) + a_u(\mathbf{u}_h, \mathbf{v}_h) + b_u(\mathbf{u}_h, \mathbf{u}_h, \mathbf{v}_h) + c_p(\mathbf{v}_h, p_h) - (\mathcal{A}_1(\psi_h, c_h), \mathbf{v}_h) \\ \quad - (b(\psi_h)((\mathbf{u}_h \times \mathbf{B}) \times \mathbf{B}), \mathbf{v}_h) = (\mathbf{F}_u, \mathbf{v}_h), \\ -c_p(\mathbf{u}_h, q_h) = 0, \\ (\partial_t \psi_h, \varphi_h) + b_\psi(\mathbf{u}_h, \psi_h, \varphi_h) + (\mathcal{A}_g(\nabla \psi_h) \nabla \psi_h, \nabla \varphi_h) + (\mathcal{A}_2(\psi_h, c_h), \varphi_h) = (F_\psi, \varphi_h), \\ (\partial_t c_h, z_h) + b_c(\mathbf{u}_h, c_h, z_h) + (D(\psi_h) \nabla c_h, \nabla z_h) + (\mathcal{A}_3(\psi_h, c_h) \nabla \psi_h, \nabla z_h) = (F_c, z_h), \\ (\mathbf{u}_h, \psi_h, c_h)(t=0) = (\mathbf{u}_{0h}, \psi_{0h}, c_{0h}). \end{array} \right. \quad (4.1)$$

Let  $(\varphi_{ih})_{1 \leq i \leq M}$ ,  $(q_{ih})_{2M+1 \leq i \leq 2M+N}$  and  $(z_{ih})_{2M+N+1 \leq i \leq 2M+N+\tilde{M}}$  be the basis of  $\mathcal{W}_h$ ,  $\mathcal{H}_h$  and  $\mathcal{M}_h$  respectively and

$$\begin{aligned} \mathbf{u}_h(x, t) &= \sum_{i=1}^M \begin{bmatrix} u_{ih}(t) \\ v_{ih}(t) \end{bmatrix} \varphi_{ih}(x) = \sum_{i=1}^M u_{ih}(t) \underline{\varphi}_{ih}^u(x) + \sum_{i=1}^M v_{ih}(t) \underline{\varphi}_{ih}^v(x), \\ p_h(x, t) &= \sum_{i=2M+1}^{2M+N} p_{ih}(t) q_{ih}(x), \quad \psi_h(x, t) = \sum_{i=2M+N+1}^{2M+N+\tilde{M}} \psi_{ih}(t) z_{ih}(x), \\ c_h(x, t) &= \sum_{i=2M+N+\tilde{M}+1}^{2M+N+2\tilde{M}} c_{ih}(t) z_{ih}(x), \end{aligned} \quad (4.2)$$

where  $\mathbf{u}_{ih} = \begin{pmatrix} u_{ih} \\ v_{ih} \end{pmatrix}$ ,  $\underline{\varphi}_{ih}^u = \begin{pmatrix} \varphi_{ih} \\ 0 \end{pmatrix}$ ,  $\underline{\varphi}_{ih}^v = \begin{pmatrix} 0 \\ \varphi_{ih} \end{pmatrix}$ .  
and  $\mathbf{v}_h$  may be represented as

$$\mathbf{v}_h = \begin{bmatrix} \varphi_{ih}(x) \\ \varphi_{ih}(x) \end{bmatrix} = \begin{bmatrix} \varphi_{ih}(x) \\ 0 \end{bmatrix} + \begin{bmatrix} 0 \\ \varphi_{ih}(x) \end{bmatrix} = \underline{\varphi}_{ih}^u(x) + \underline{\varphi}_{ih}^v(x) \quad (4.3)$$

In order to derive the numerical scheme, first few terms have been elaborated subsequently. Making use of (4.2) and (4.3), the first term  $\rho_0 (\partial_t \mathbf{u}_h, \mathbf{v}_h)$  in the first equation of weak formulation (4.1) yields

$$\begin{aligned} \rho_0 (\partial_t \mathbf{u}_h, \mathbf{v}_h) &= \rho_0 \left( \sum_{i=1}^M \frac{du_{ih}(t)}{dt} \underline{\varphi}_{ih}^u(x) + \sum_{i=1}^M \frac{dv_{ih}(t)}{dt} \underline{\varphi}_{ih}^v(x), \underline{\varphi}_{ih}^u(x) + \underline{\varphi}_{ih}^v(x) \right) \\ &= \rho_0 \sum_{i=1}^M \left( \underline{\varphi}_{ih}^u(x), \underline{\varphi}_{ih}^u(x) \right) \frac{du_{ih}(t)}{dt} + \rho_0 \sum_{i=1}^M \left( \underline{\varphi}_{ih}^v(x), \underline{\varphi}_{ih}^v(x) \right) \frac{dv_{ih}(t)}{dt} \end{aligned}$$

Consider the second term

$$\begin{aligned} a_u(\mathbf{u}_h, \mathbf{v}_h) &= a_u \left( \sum_{i=1}^M u_{ih}(t) \underline{\varphi}_{ih}^u(x) + \sum_{i=1}^M v_{ih}(t) \underline{\varphi}_{ih}^v(x), \underline{\varphi}_{ih}^u(x) + \underline{\varphi}_{ih}^v(x) \right) \\ &= \sum_{i=1}^M a_u \left( \underline{\varphi}_{ih}^u(x), \underline{\varphi}_{ih}^u(x) \right) u_{ih}(t) + \sum_{i=1}^M a_v \left( \underline{\varphi}_{ih}^v(x), \underline{\varphi}_{ih}^v(x) \right) v_{ih}(t) \end{aligned}$$

and third term can be obtained in a similar manner as

$$\begin{aligned} b_u(\mathbf{u}_h, \mathbf{u}_h, \mathbf{v}_h) &= b_u \left( \mathbf{u}_h, \sum_{i=1}^M u_{ih}(t) \underline{\varphi}_{ih}^u(x) + \sum_{i=1}^M v_{ih}(t) \underline{\varphi}_{ih}^v(x), \underline{\varphi}_{ih}^u(x) + \underline{\varphi}_{ih}^v(x) \right) \\ &= b_u \left( \mathbf{u}_h, \sum_{i=1}^M u_{ih}(t) \underline{\varphi}_{ih}^u(x), \underline{\varphi}_{ih}^u(x) \right) + b_u \left( \mathbf{u}_h, \sum_{i=1}^M v_{ih}(t) \underline{\varphi}_{ih}^v(x), \underline{\varphi}_{ih}^v(x) \right) \\ &= \sum_{i=1}^M b_u \left( \mathbf{u}_h, \underline{\varphi}_{ih}^u(x), \underline{\varphi}_{ih}^u(x) \right) u_{ih}(t) + \sum_{i=1}^M b_u \left( \mathbf{u}_h, \underline{\varphi}_{ih}^v(x), \underline{\varphi}_{ih}^v(x) \right) v_{ih}(t) \end{aligned}$$

Substituting above expressions into the first equation of weak form (4.1) and using (4.2) and (4.3), the semi-discrete weak form yields

$$\begin{aligned}
& \sum_{i=1}^M \rho_0 \left( \underline{\varphi}_{ih}^u, \underline{\varphi}_{jh}^u \right) \frac{d u_{ih}}{dt} + \sum_{i=1}^M \left( a_u \left( \underline{\varphi}_{ih}^u, \underline{\varphi}_{jh}^u \right) + b_u \left( \mathbf{u}_h, \underline{\varphi}_{ih}^u, \underline{\varphi}_{jh}^u \right) \right. \\
& \quad \left. - \left( b(\psi_h) \left( (\underline{\varphi}_{ih}^u \times \mathbf{B}) \times \mathbf{B} \right), \underline{\varphi}_{jh}^u \right) \right) u_{ih} + \sum_{i=2M+1}^{2M+N} \left( q_{ih}, \operatorname{div}(\underline{\varphi}_{jh}^u) \right) p_{ih} \\
& \quad - \left( \mathcal{A}_1(\psi_h, c_h), \underline{\varphi}_{jh}^u \right) + \sum_{i=1}^M \rho_0 \left( \underline{\varphi}_{ih}^v, \underline{\varphi}_{jh}^v \right) \frac{d v_{ih}}{dt} \\
& \quad + \sum_{i=1}^M \left( a_u \left( \underline{\varphi}_{ih}^v, \underline{\varphi}_{jh}^v \right) + b_u \left( \mathbf{u}_h, \underline{\varphi}_{ih}^v, \underline{\varphi}_{jh}^v \right) \right. \\
& \quad \left. - \left( b(\psi_h) \left( (\underline{\varphi}_{ih}^v \times \mathbf{B}) \times \mathbf{B} \right), \underline{\varphi}_{jh}^v \right) \right) v_{ih} + \sum_{i=2M+1}^{2M+N} \left( q_{ih}, \operatorname{div}(\underline{\varphi}_{jh}^v) \right) p_{ih} \\
& \quad - \left( \mathcal{A}_1(\psi_h, c_h), \underline{\varphi}_{jh}^v \right) = \left( \mathbf{F}_u, \underline{\varphi}_{jh}^u + \underline{\varphi}_{jh}^v \right), \quad \text{for all } 1 \leq j \leq M, \\
& \quad - \sum_{i=2M+1}^{2M+N} \left\{ \left( \operatorname{div}(\underline{\varphi}_{ih}^u), q_{jh} \right) u_{ih} + \left( \operatorname{div}(\underline{\varphi}_{ih}^v), q_{jh} \right) v_{ih} \right\} = 0, \quad 2M+1 \leq j \leq 2M+N, \\
& \quad \sum_{i=2M+N+1}^{2M+N+\tilde{M}} (z_{ih}, z_{jh}) \frac{d \psi_{ih}}{dt} + \sum_{i=2M+N+1}^{2M+N+\tilde{M}} \left\{ b_\psi \left( \mathbf{u}_h, z_{ih}, z_{jh} \right) + \left( \mathcal{A}_g(\nabla \psi_h) \nabla z_{ih}, \nabla z_{jh} \right) \right\} \psi_{ih} \\
& \quad + \left( \mathcal{A}_2(\psi_h, c_h), z_{jh} \right) = \left( F_\psi, z_{jh} \right), \quad \text{for all } 2M+N+1 \leq j \leq 2M+N+\tilde{M}, \\
& \quad \sum_{i=2M+N+\tilde{M}+1}^{2M+N+2\tilde{M}} (z_{ih}, z_{jh}) \frac{d c_{ih}}{dt} + \sum_{i=2M+N+\tilde{M}+1}^{2M+N+2\tilde{M}} \left\{ b_c \left( \mathbf{u}_h, z_{ih}, z_{jh} \right) \right. \\
& \quad \left. + \left( D(\psi_h) \nabla z_{ih}, \nabla z_{jh} \right) \right\} c_{ih} + \sum_{i=2M+N+1}^{2M+N+\tilde{M}} \left( \mathcal{A}_3(\psi_h, c_h) \nabla z_{ih}, \nabla z_{jh} \right) \psi_{ih} \\
& \quad = \left( F_c, z_{jh} \right), \quad \text{for all } 2M+N+\tilde{M}+1 \leq j \leq 2M+N+2\tilde{M}.
\end{aligned}$$

These equations can be written in the differential-algebraic system form (DAE) as

$$\begin{aligned}
\mathbb{M} \frac{d \mathbf{Y}^h}{dt} + \mathbb{A}(\mathbf{Y}^h) \mathbf{Y}^h + \mathbf{L}(\mathbf{Y}^h) &= \mathbf{R}, \quad \mathbf{Y}^h(t=0) = \mathbf{Y}_0^h, \\
\mathbf{Y}^h &= \left( \mathbf{u}_{1h} \cdots \mathbf{u}_{Mh} \quad p_{1h} \cdots p_{Nh} \quad \psi_{1h} \cdots \psi_{\tilde{M}h} \quad c_{1h} \cdots c_{\tilde{M}h} \right)^t,
\end{aligned} \tag{4.4}$$

where  $\mathbf{R} = (R_1 \ 0 \ R_3 \ R_4)^t$ ,  $\mathbf{L}(Y_h) = (L_1 \ 0 \ L_3 \ 0)^t$  and, for  $K_1 = 2M+N+2\tilde{M}$  and  $K_2 = 2M+N+2\tilde{M}$

$$\mathbb{M} = \begin{pmatrix} M_{11} & 0 & 0 & 0 \\ 0 & 0 & 0 & 0 \\ 0 & 0 & M_{33} & 0 \\ 0 & 0 & 0 & M_{44} \end{pmatrix} \in \mathbb{R}^{K_1, K_2}, \quad \mathbb{A}(\mathbf{Y}_h) = \begin{pmatrix} A_{11} & A_{12} & 0 & 0 \\ A_{21} & 0 & 0 & 0 \\ 0 & 0 & A_{33} & 0 \\ 0 & 0 & A_{43} & A_{44} \end{pmatrix} \in \mathbb{R}^{K_1, K_2},$$

with

$$\begin{aligned}
(M_{11})_{ji} &= \rho_0 \left( \underline{\varphi}_{ih}^u, \underline{\varphi}_{jh}^u \right) + \rho_0 \left( \underline{\varphi}_{ih}^v, \underline{\varphi}_{jh}^v \right), & (M_{33})_{ji} &= (z_{ih}, z_{jh}), & (M_{44})_{ji} &= (z_{ih}, z_{jh}), \\
(A_{11})_{ji} &= a_u \left( \underline{\varphi}_{ih}^u, \underline{\varphi}_{jh}^u \right) + a_u \left( \underline{\varphi}_{ih}^v, \underline{\varphi}_{jh}^v \right) + b_u \left( \mathbf{u}_h, \underline{\varphi}_{ih}^u, \underline{\varphi}_{jh}^u \right) + b_u \left( \mathbf{u}_h, \underline{\varphi}_{ih}^v, \underline{\varphi}_{jh}^v \right) \\
&\quad - \left( b(\psi_h) \left( (\underline{\varphi}_{ih}^u \times \mathbf{B}) \times \mathbf{B} \right), \underline{\varphi}_{jh}^u \right) - \left( b(\psi_h) \left( (\underline{\varphi}_{ih}^v \times \mathbf{B}) \times \mathbf{B} \right), \underline{\varphi}_{jh}^v \right), \\
(A_{12})_{ji} &= \left( q_{ih}, \nabla \cdot (\underline{\varphi}_{jh}^u) \right) + \left( q_{ih}, \nabla \cdot (\underline{\varphi}_{jh}^v) \right) = (A_{21})_{ij}, \\
(A_{33})_{ji} &= (\mathcal{A}_g(\nabla \psi_h) \nabla z_{ih}, \nabla z_{jh}) + b_\psi(\mathbf{u}_h, z_{ih}, z_{jh}), \\
(A_{43})_{ji} &= (\mathcal{A}_2(\psi_h, c_h) \nabla z_{ih}, \nabla z_{jh}), & (A_{44})_{ji} &= (D(\psi_h) \nabla z_{ih}, \nabla z_{jh}) + b_c(\mathbf{u}_h, z_{ih}, z_{jh}), \\
(L_1)_j &= \left( \mathcal{A}_1(\psi_h, c_h), \underline{\varphi}_{jh}^u \right) + \left( \mathcal{A}_1(\psi_h, c_h), \underline{\varphi}_{jh}^v \right), & (L_3)_j &= \epsilon_1 (\mathcal{A}_2(\psi_h, c_h), z_{jh}), \\
(R_1)_j &= \left( \mathbf{F}_u, \underline{\varphi}_{jh}^u \right) + \left( \mathbf{F}_u, \underline{\varphi}_{jh}^v \right), & (R_3)_j &= (F_\psi, z_{jh}), & (R_4)_j &= (F_c, z_{jh}).
\end{aligned} \tag{4.5}$$

The equation (4.4) can be written in general form as

$$\mathcal{F}(t, \mathbf{Y}^h(t), \frac{d\mathbf{Y}^h}{dt}) = 0, \quad \mathbf{Y}^h(t=0) = \mathbf{Y}_0^h. \tag{4.6}$$

In order to consider the fully discrete scheme, for an integer  $K > 0$ , we introduce the timestep  $\tau = \frac{T}{K}$ , the time subdivision  $t_i = i\tau$  ( $0 \leq i \leq K$ ) of  $[0, T]$  and, for sufficiently regular function  $\mathbf{v}$ , we denote by  $\mathbf{v}_i$  the value of  $\mathbf{v}$  at time  $t_i$  and by  $\partial_{\tau, n} \mathbf{v} = \frac{\mathbf{v}_{n+1} - \mathbf{v}_n}{\tau}$ .

The differential-algebraic system (4.4) is first fully discretized by invoking Euler's backward difference method as

$$\mathcal{F}(t_{n+1}, \mathbf{Y}_{n+1}^h, \partial_{\tau, n} \mathbf{Y}^h) = 0 \tag{4.7}$$

and then solved by employing the Newton iteration technique on the resulting non-linear fixed-point system, for this purpose we have used the solver DASSL [13].

Then, the following a priori error estimates for the solution  $(\Psi_h, p_h)$ , with  $\Psi_h = (\mathbf{u}_h, \psi_h, c_h)$ , of the finite element discretization (4.7) can be obtained by using the assumptions (C1)-(C5) and method as those in e.g. [4, 26] (for some  $\beta_1, \beta_2 > 1$  and  $\alpha \geq 1$ )

$$\|\Psi_h - \Psi\|_{\ell^2(0, T, L^2(\Omega))} \leq C_\delta(\tau^\alpha + h^{\beta_1}) \text{ and } \|p_h - p\|_{\ell^2(0, T, L^2(\Omega))} \leq C_\delta(\tau^\alpha + h^{\beta_2}) \tag{4.8}$$

where  $C_\delta > 0$  is independent of  $h$ ,  $\Psi = (\mathbf{u}, \psi, c)$  is the known exact solution of the problem under consideration and the space  $\ell^p(0, T, \mathbb{X})$ , for a Banach space  $\mathbb{X}$  and  $0 < p < +\infty$  is defined by

$$\ell^p(0, T, \mathbb{X}) = \left\{ \mathbf{v} : (t_1, \dots, t_k) \rightarrow \mathbb{X} \text{ such that } \|\mathbf{v}\|_{\ell^p(0, T, \mathbb{X})} = \left( \tau \sum_{i=1}^k \|\mathbf{v}_i\|_{\mathbb{X}}^p \right)^{1/p} < \infty \right\}.$$

In the next section, we shall present the results (4.8) in order to validate the error analysis and stability of numerical scheme by by considering some examples.

## 5 Analysis of the numerical scheme

We shall discuss error analysis of the scheme with the help of numerical examples to verify theoretical estimates (4.8) and stability of the method. To obtain the convergence rates of the derived scheme, two numerical tests are conducted: the first compute the time discretization error, and the second calculate the spatial discretization error. In order to validate the numerical stability of the method, we incorporated  $(1 - \epsilon \text{ randf})$  on the right hand side terms to introduce perturbations by introducing  $\epsilon$  in the numerical solution, where  $\text{randf}$  denotes random function (that generates some F-distributed random variables) assumes values in  $[0, 1]$  and  $\epsilon$  is parameter to control perturbation. The parameters are same as given in [31] and the constants for the meltflow equations are taken in view of the physical properties of the nickelcopper (NiCu) system see Table 1 (see e.g., [20]).

As exact solutions, we consider the two following examples (with  $T = 1$  and  $\mathbf{B} = \frac{1}{\sqrt{2}}(1, 1)$ ).

Property Name	Symbol	Unit	Nickel (A)	Copper (B)
Melting temperature	$T_m$	$K$	1728	1358
Latent heat	$L$	$J/m^3$	$2350 \times 10^6$	$1758 \times 10^6$
Diffusion coeff. liquid	$D_L$	$m^2/s$	$10^{-9}$	$10^{-9}$
Diffusion coeff. solid	$D_S$	$m^2/s$	$10^{-13}$	$10^{-13}$
Linear kinetic coeff.	$\beta$	$m/K/s$	$3.3 \times 10^{-3}$	$3.9 \times 10^{-3}$
Interface thickness	$\delta$	$m$	$8.4852 \times 10^{-8}$	$6.0120 \times 10^{-8}$
Density	$\rho$	$Kg/m^3$	7810	8020
viscosity	$\mu$	$Pa \cdot s$	$4.110 \times 10^{-6}$	$0.597 \times 10^{-6}$
Surface energy	$\sigma$	$J/m^2$	0.37	0.29
Electrical conductivity	$\sigma_e$	$S/m$	$14.3 \times 10^6$	$59.6 \times 10^6$
Molar volume	$V_m$	$m^3$	$7.46 \times 10^{-6}$	$7.46 \times 10^{-6}$
Mode Number	$k$	N/A	4	4
Anisotropy Amplitude	$\gamma_0$	N/A	0.04	0.04

Table 1: Physical values of constants

- Example 1 :

$$\begin{aligned}
u_{ex}(x, y, t) &= \frac{2}{(2\pi)^2} e^{1-t} \sin(x)^2 y \left(1 - \frac{y}{2\pi}\right) \left(1 - \frac{y}{\pi}\right), \\
v_{ex}(x, y, t) &= -\frac{2}{(2\pi)^2} e^{1-t} \sin(x) \cos(x) y^2 \left(1 - \frac{y}{2\pi}\right)^2, \quad p_{ex}(x, y, t) = e^{1-t} \cos(y), \\
\psi_{ex}(x, y, t) &= \frac{e^{1-t}}{2} (\cos(x) \cos(y) + 1), \quad c_{ex}(x, y, t) = \frac{8}{(2\pi)^2} e^{1-t} x^2 \left(1 - \frac{x}{2\pi}\right)^2 (\cos(y) + 1),
\end{aligned} \tag{5.1}$$

where  $\Omega = [0, 2\pi] \times [0, 2\pi]$ .

- Example 2 :

$$\begin{aligned}
u_{ex}(x, y, t) &= 4\pi e^{t-1} x^2 (1-x)^2 \sin(2\pi y) \cos(2\pi y), \\
v_{ex}(x, y, t) &= -2e^{t-1} x(2x^2 - 3x + 1) \sin^2(2\pi y), \quad p_{ex}(x, y, t) = e^{t-1} \cos(2\pi x), \\
\psi_{ex}(x, y, t) &= \frac{1}{4} e^{t-1} (\cos(2\pi x) + \cos(2\pi y) + 2), \quad c_{ex}(x, y, t) = 8e^{t-1} (x^2(1-x)^2 + y^2(1-y)^2),
\end{aligned} \tag{5.2}$$

where  $\Omega = [0, 1] \times [0, 1]$ .

The terms  $\mathbf{F}_u$ ,  $F_\psi$  and  $F_c$  on right hand sides are computed carefully to ensure that (5.1) (resp. (5.2)) is the exact solution of system (2.1). We consider four meshes with step size  $h$  (see Fig.1 and Table 2).

Mesh	$h$	Elements	Boundary elements
1.0	0.20	106.0	5.0
2.0	0.150	200.0	7.0
3.0	0.10	434.0	10.0
4.0	0.050	1712.0	20.0

Table 2: Mesh Statistics

## 5.1 Numerical error analysis

In order to validate the error estimates numerically and the convergence orders of scheme, two types of computations have been made. First, we have computed the convergence rates with respect to apatial coordinates wherein sufficiently small timesteps  $\tau$  (as compared to the spatial step size  $h$ ) are fixed and we have varied the spatial step size  $h$  as described in Table 2 of mesh statistics. The rates  $\beta_1$  and  $\beta_2$  have been calculated with respect to  $h$  and we use the Lagrange-quadratic  $\mathbb{P}_2$  and Lagrange-cubic  $\mathbb{P}_3$  finite elements for the phase-field and concentration system, and the velocity/pressure mixed finite elements  $\mathbb{P}_2 - \mathbb{P}_1$  and  $\mathbb{P}_3 - \mathbb{P}_2$  for the melt flow system.

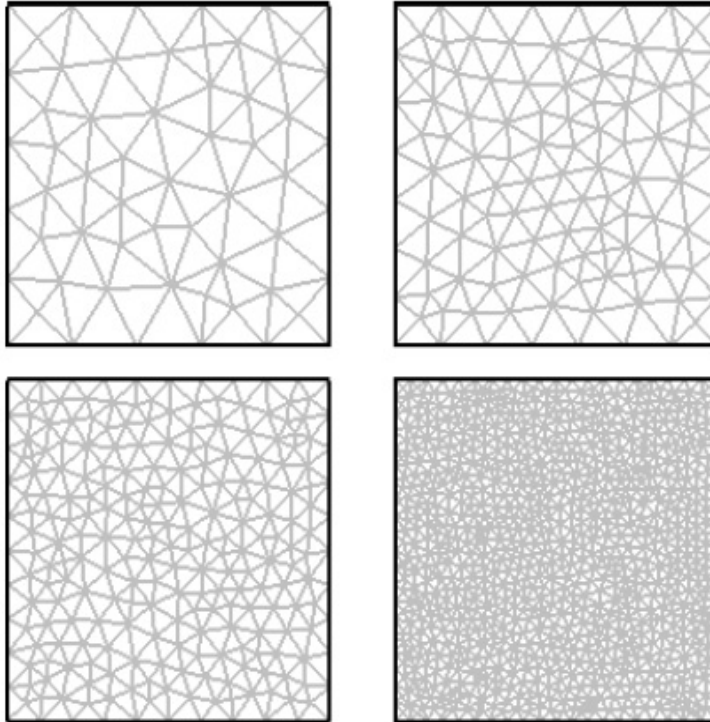


Figure 1: Meshes

The Fig. 2 and Fig. 3 represent the  $L^2(\mathcal{Q})$ -norms of errors of  $\mathbf{u}$ ,  $p$ ,  $\psi$  and  $c$  which are plotted versus  $h$  and  $\tau$  respectively, in  $\log$ -scales. For  $h$ -curves, we use  $\tau = 0.01$ ,  $\tau = 0.001$  and  $\tau = 0.0001$  for linear, quadratic and cubic polynomials, respectively. It is to be noted that the slopes of error curves are approximately equal to 3 and 4 for quadratic and cubic finite elements respectively for the velocity, phase-field and concentration, whereas the slopes of error curves for the pressure are approximately equal to 2 and 3 for linear and quadratic finite elements respectively; refer to Table 3 and Table 4.  $\tau$ -curves slopes of all the curves are approximately 1, i.e.,  $\alpha = 1$ ; refer to Table 5 and Table 6. Both numerical estimates are in an excellent agreement with error estimates (4.8).

	Error Estimate	$\mathbf{P}_2 - \mathbf{P}_1$	$\mathbf{P}_3 - \mathbf{P}_2$
Example 1	$\beta_1$ for $\mathbf{u}$	2.6201	3.8730
	$\beta_2$ for $p$	1.9207	3.0646
Example 2	$\beta_1$ for $\mathbf{u}$	2.7664	4.0303
	$\beta_2$ for $p$	2.3462	3.4302

Table 3: Order of convergence  $\beta_i$ , ( $i = 1, 2$ ), for velocity  $\mathbf{u}$  and pressure  $p$  in Examples 1 and 2.

## 5.2 Numerical stability analysis

An extra term  $(1 - \epsilon \text{randf})$  has been incorporated in the right hand side terms of each equation in (4.7) to introduce  $\epsilon$ -perturbations, where  $\text{randf}$  assumes values in  $[0, 1]$  (see e.g. Fig. 4) and  $\epsilon$  is the perturbation control parameter. We fix  $h = 0.2$  and  $\tau = 0.1$  and we use quadratic finite elements  $\mathbb{P}_2$  for  $\psi$ ,  $c$  and  $\mathbf{u}$  and linear finite elements  $\mathbb{P}_1$  for  $p$  in order to study the stability of the method. We perform three different

	Error Estimate	$\mathbf{P}_2$	$\mathbf{P}_3$
Example 1	$\beta_1$ for $\psi$	2.7001	3.7500
	$\beta_1$ for $c$	2.9278	3.8739
Example 2	$\beta_1$ for $\psi$	2.9200	3.8200
	$\beta_1$ for $c$	2.8972	4.0681

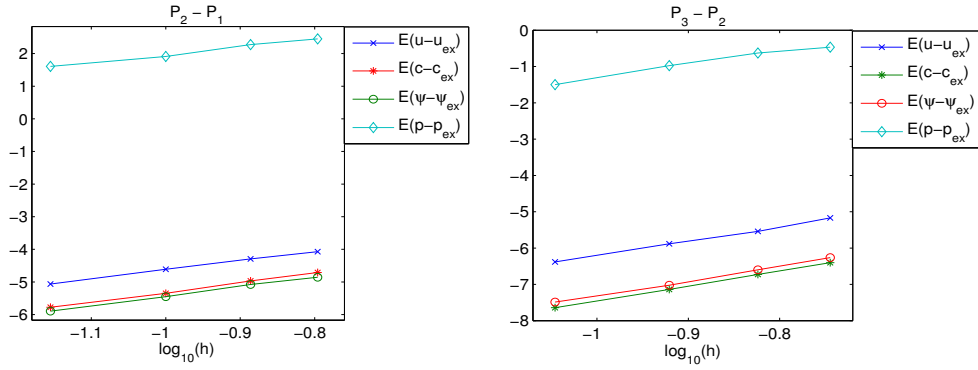
Table 4: Order of convergence  $\beta_1$  for phase-field  $\psi$  and concentration  $c$  in Examples 1 and 2.

	Error Estimate	$\mathbf{P}_2 - \mathbf{P}_1$	$\mathbf{P}_3 - \mathbf{P}_2$
Example 1	$\alpha$ for $\mathbf{u}$	1.1494	1.1446
	$\alpha$ for $p$	1.0733	1.0634
Example 2	$\alpha$ for $\mathbf{u}$	0.9011	0.9152
	$\alpha$ for $p$	1.0032	0.9944

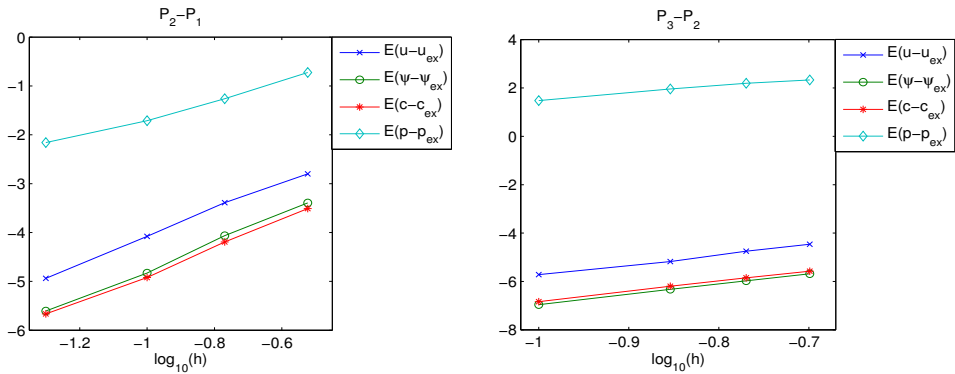
Table 5: Order of convergence  $\alpha$  for velocity  $\mathbf{u}$  and pressure  $p$  in Examples 1 and 2.

computational stability tests (in Fig.5, Fig.6, Fig.7 and Fig.8).

In Fig. 5, the  $L^2(Q)$ -norm of the discrepancy between exact solution  $\Phi_{ex} = (\Phi_{ex}^{(s)})_{s=1,4} = (\mathbf{u}_{ex}, p_{ex}, \psi_{ex}, c_{ex})$  and its  $\epsilon$ -perturbation  $\Phi_\epsilon = (\Phi_\epsilon^{(s)})_{s=1,4} = (\mathbf{u}_\epsilon, p_\epsilon, \psi_\epsilon, c_\epsilon)$  i.e.  $E_{\epsilon,ex}(\Phi_\epsilon^{(s)} - \Phi_{ex}^{(s)}) = \left\| \Phi_\epsilon^{(s)} - \Phi_{ex}^{(s)} \right\|_{L^2(Q)}$ , for

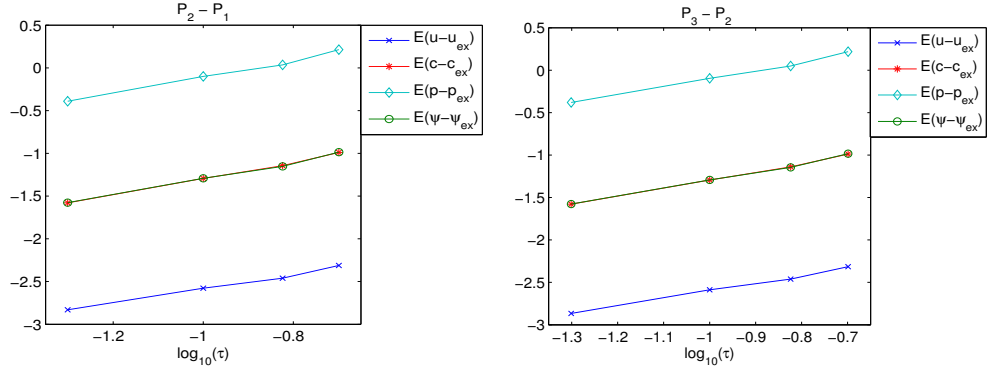


(a) Spatial error curves in Example 1

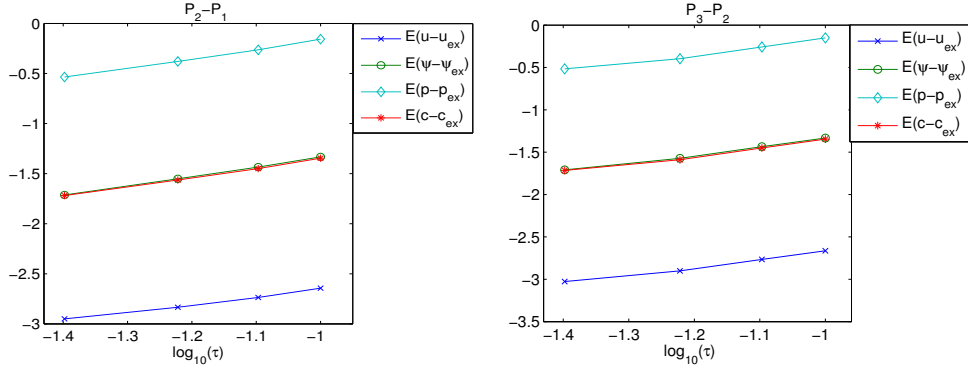


(b) Spatial error curves in Example 2

Figure 2: Error curves with respect to spatial step  $h$  obtained in Examples 1 and 2.



(a) Temporal error curves in Example 1



(b) Temporal error curves in Example 2

Figure 3: Error curves with respect to temporal step  $\tau$  obtained in Examples 1 and 2.

	Error Estimate	$\mathbf{P}_2$	$\mathbf{P}_3$
Example 1	$\alpha$ for $\psi$	1.0558	1.0396
	$\alpha$ for $c$	1.0602	1.0565
Example 2	$\alpha$ for $\psi$	0.9821	0.9856
	$\alpha$ for $c$	0.9792	0.9815

Table 6: Order of convergence  $\alpha$  for phase-field  $\psi$  and concentration  $c$  in Examples 1 and 2.

$s = 1, 4$  are plotted versus  $\epsilon$  (which are shown for  $\epsilon = 0.01, 0.05, 0.1, 0.15, 0.2, 0.3, 0.4$ ). A linear dependence of errors on  $\epsilon$  is observed, indeed,  $E_{\epsilon,ex}(\Phi_\epsilon^{(s)} - \Phi_{ex}^{(s)}) \approx m_s \epsilon$ , for  $s = 1, 4$ , where  $m_s$  represents the slope of the error curve; refer to Table 7. In Fig. 6, the error  $E_{\epsilon,app}(\Phi_\epsilon^{(s)} - \Phi_{app}^{(s)}) = \|\Phi_\epsilon^{(s)} - \Phi_{app}^{(s)}\|_{L_2(Q)}$ , for  $s = 1, 4$  between the approximate solution  $\Phi_{app} = (\Phi_{app}^{(s)})_{s=1,4} = (\mathbf{u}_{app}, p_{app}, \psi_{app}, c_{app})$  without random (i.e.,  $\epsilon = 0$ ) and  $\Phi_\epsilon$ , are plotted against  $\epsilon$ . The same observation holds as in Fig. 5; refer also to Table 7.

Finally, in Fig. 7 and Fig. 8, the solutions are shown on a part of domain and at time  $t = 1$  in order demonstrate stability with respect to perturbations. In Fig. 7, we fix  $y = \pi/2$  and  $x$  varies for velocity and concentration, and  $t = 1$ ,  $x = \pi$  and  $y$  varies for pressure and phase field. In Fig. 8 we fix  $x = 1/2$  and  $y$  varies for velocity and phase field, and  $x = 1/2$  and  $y$  varies. The graphs shows that the solution is stable.

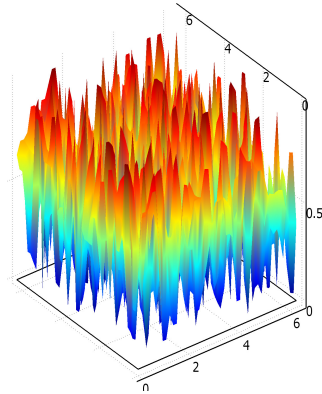
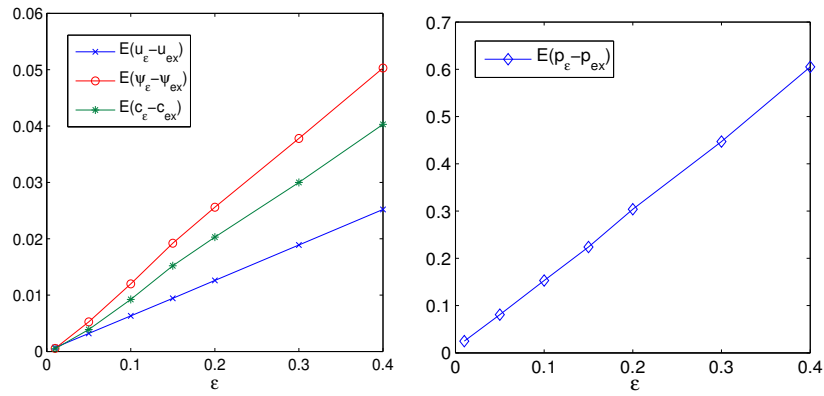
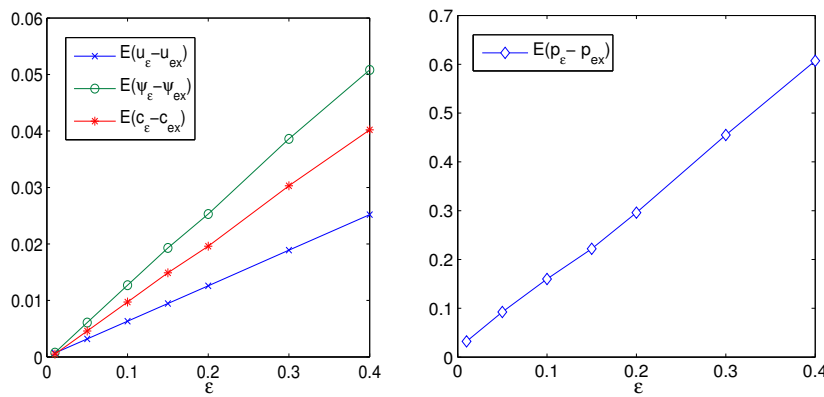


Figure 4: Random function.



(a) Error curves in Example 1

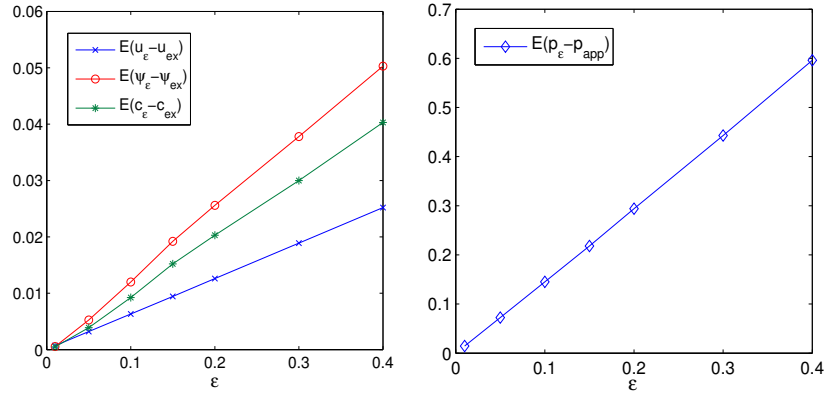


(b) Error curves in Example 2

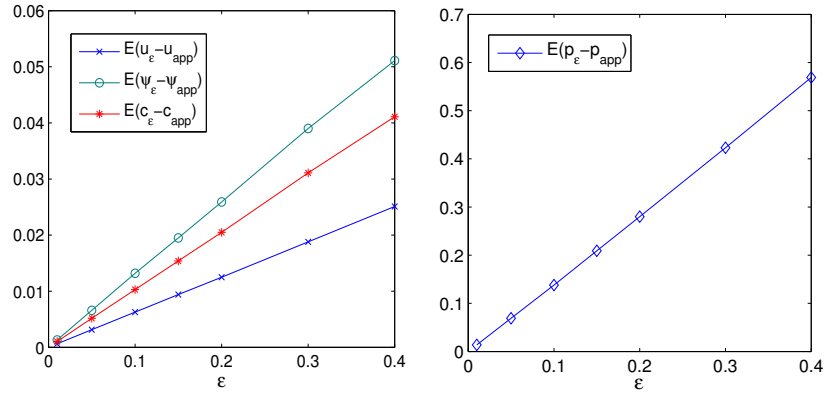
Figure 5: Errors Curves of norm  $EE_{\epsilon,ex}$ .

## 6 Concluding remarks

This paper presents a numerical investigation and resolution of the isothermal anisotropic solidification model (2.1). The purpose of this study is to validate the derived numerical scheme by performing its error



(a) Error curves in Example 1



(b) Error curves in Example 2

Figure 6: Errors Curves of norm  $E_{\epsilon,app}$ .

	Slope	$E_{\epsilon,ex}$	$E_{\epsilon,app}$
Example 1	$m_{\mathbf{u}}$	0.1701	0.1754
	$m_{\psi}$	0.8638	0.8818
	$m_c$	0.4341	0.4371
	$m_p$	1.4738	1.4913
Example 2	$m_{\mathbf{u}}$	0.0628	0.0635
	$m_{\psi}$	0.1283	0.1347
	$m_c$	0.1018	0.1065
	$m_p$	1.4877	1.4236

Table 7: Slopes of Norm  $L_2$  in Examples 1 and 2.

and stability analysis. The model has been discretized with respect to spatial and time variables. The discretization result into a system of nonlinear ordinary differential equations. The resulting non-linear systems are solved by using a solver DASSL.

Second, the convergence and stability of the numerical scheme has been validated (both with respect to space and time variables) by considering two examples with known exact solutions. It is numerically demonstrated that the error estimates with respect to spatial coordinates are of order  $i + 1$  for  $\mathbf{u}$ ,  $\psi$  and  $c$  and of order  $i$  for  $p$ , and the error estimates for time are of order 1 for  $(\mathbf{u}, p, \psi, c)$ . Both of these numerical estimates are in excellent accordance with the estimates (4.8). The stability of the scheme has also been

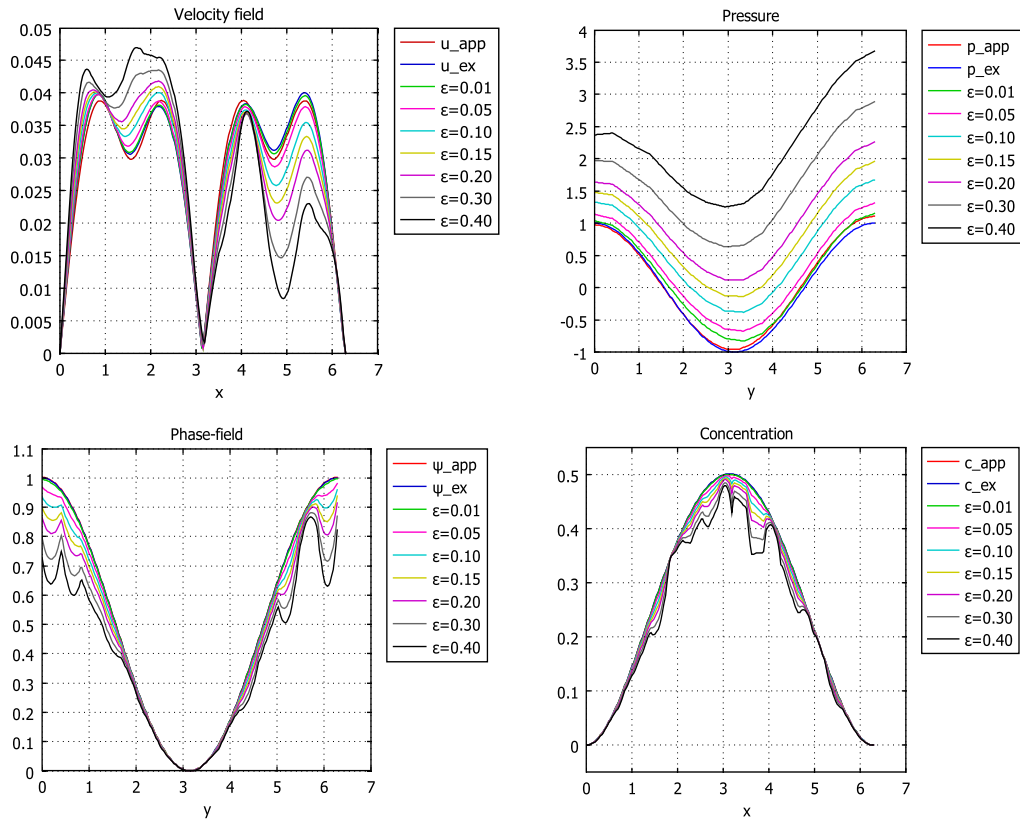


Figure 7: Solution curves for the different values of  $\epsilon$  in Example 2.

verified by introducing a random function, which varies between 0 and 1, in the model. It is found that the numerical scheme is completely stable and it has linear dependence with the increase in percentage error.

## 7 Declarations

**Competing interests:** The author declare that he has no competing interests.

**Acknowledgments:** The author is thankful to the journal for consideration of this manuscript.

## References

- [1] Zhu M. F., Ting D., Lee S. Y. and Hong C. P., “Modeling of solutal dendritic growth with melt convection”, *Computers and Mathematics with Applications*, Vol. **55**, pp. 1620-1628, 2008. **1**
- [2] Sun D. K., Zhu M.F., Pan S.Y., Yang C.R. and Raabe D., “Lattice Boltzmann modeling of dendritic growth in forced and natural convection”, *Computers and Mathematics with Applications*, Vol. **61**, pp. 3585-3592, 2011. **1**
- [3] Anderson D. M., McFadden G. B., Wheeler A. A., “A phase-field model of solidification with convection”, *Physica D*, Vol. **135**, pp. 175-194, 2000. **1**
- [4] Belmiloudi A., “Method of characteristics and error estimates of the perturbation of given mean flow. Application of mathematics in Engineering and Business Sozopol”, *Proceedings of the XXII Summer School*, pp. 25-38, 1996. **4, 7**

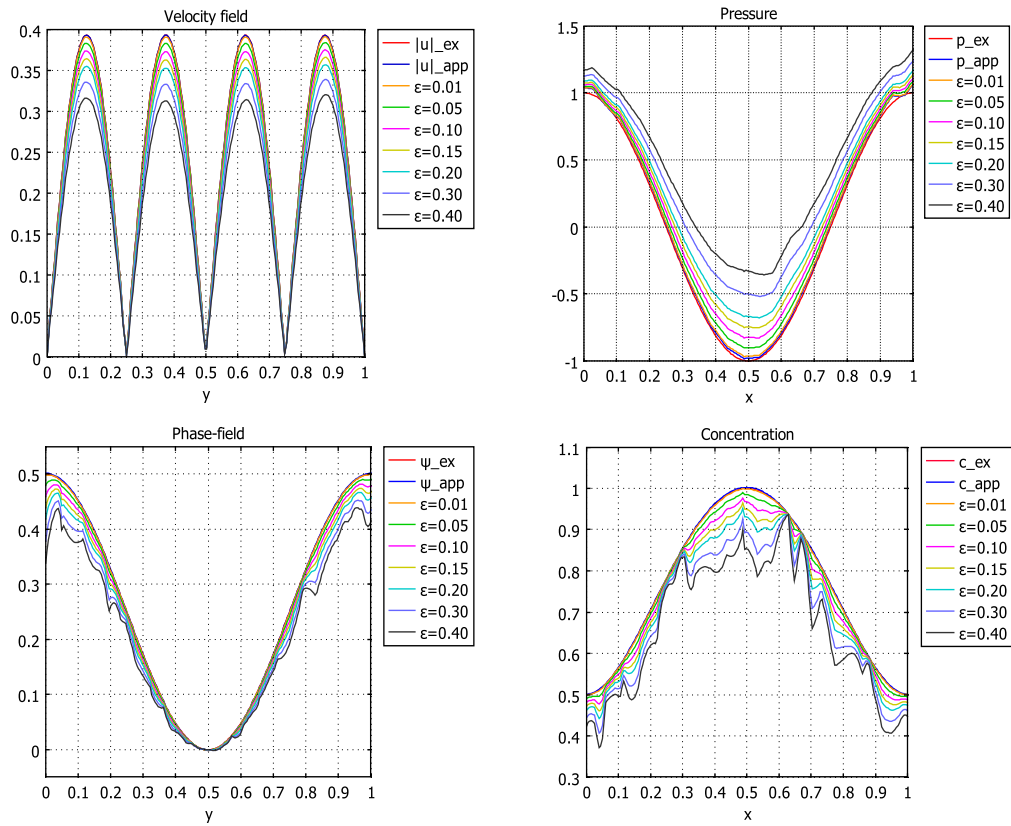


Figure 8: Solution curves for the different values of  $\epsilon$  in Example 1.

- [5] Belmiloudi A., “Robin-type boundary control problems for the nonlinear Boussinesq type equations”, *Journal of Mathematical Analysis & Applications*, Vol. **273**, pp. 428-456, 2002. **3**
- [6] Belmiloudi A., “Robust and optimal control problems to a phase-field model for the solidification of a binary alloy with a constant temperature”, *Journal of Dynamical & Control Systems*, Vol. **10**, pp. 453-499, 2004. **1**
- [7] Belmiloudi A., “Stabilization, optimal and robust control: Theory and Applications in Biological and Physical Systems”, Springer-Verlag, London, Berlin, 2008. **1**
- [8] Chen Z., Hoffmann K. H., “An error estimate for a finite-element scheme for a phase field model”, *IMA J. Numer. Anal.*, Vol. **14**, pp. 243-255, 1994.
- [9] Galindo V., Gerbeth G., Ammon W. V., Tomzig E., Virbulis J., “Crystal growth melt flow previous term control next term by means of magnetic fields”, *Energy Conv. Manage.* Vol. **43**, pp. 309-316, 2002. **1**
- [10] Grujicic M., Cao G., Millar R. S., “Computer modelling of the evolution of dendrite microstructure in binary alloys during non-isothermal solidification”, *J. Materials synthesis and processing*, Vol. **10**, No. 4, 191-203, 2002. **1**
- [11] Gunzberger M., Ozugurlu E., Turner J., Zhang H., “Controlling transport phenomena in the Czochralski crystal growth process”, *J. Crystal Growth*, Vol. **234**, pp. 47-62, 2002. **1**
- [12] Hadid H. B., Henry D., Kaddeche S., “Numerical study of convection in the horizontal Bridgman configuration under the action of a constant magnetic field. Part 1. Two dimensional flow”, *J. Fluid Mech.*, Vol. **333**, pp. 23-56, 1997. **1**

- [13] Petzold L. R., "A discription of DASSL: A differential/algebraic system solver", *Scientific computing, IMACS Trans. Sci. Comput.*, pp. 65-68, 1983. [7](#)
- [14] Li M., Takuya T., Omura N., Miwa K., "Effects of magnetic field and electric current on the solidification of AZ91D magnesium alloys using an electromagnetic vibration technique", *J. of Alloys and Compounds*, Vol. **487**, pp. 187-193, 2009. [1](#)
- [15] Ramizer J. C., Beckermann C., Kerma A., Diepers H. J., "Phase-field modeling of binary alloy solidification with couple heat and solute diffusion", *Physical Review E*, Vol **69**, pp. (051607-1)-(051607-16), 2004. [1](#)
- [16] Ramizer J. C., Beckermann C., "Examination of binary alloy free dendritic growth theories with a phase-field model", *Acta Materialia*, Vol. **53**, pp. 1721-1736, 2005. [1](#)
- [17] Rappaz M., Rettenmayr M., "Simulation of solidification", *Current Opinion in Solid State and Materials Science*, Vol. **3**, pp. 275-282, 1998. [1](#)
- [18] Rasheed A., Belmiloudi A., Mahe F., "Dynamics of dendrite growth in a binary alloy with magnetic field affect", *Discrete and Continuous Dynamical Systems*, Vol. **2011**, pp. 1224-1233, Special Issue, 2011. [1](#)
- [19] Rasheed A., Belmiloudi A., "An analysis of the Phase-field model for isothermal binary alloy solidification with convection under the influence of magnetic field", *Journal of Mathematical Analysis & Applications*, Vol. **390**, pp. 244-273, 2012. [1](#)
- [20] Rasheed A., Belmiloudi A., "Mathematical Modelling and Numerical Simulation of Dendrite Growth Using Phase-Field Method with a Magnetic Field Effect", *Communications in Computational Physics*, Vol. **14**, pp. 477-508, 2013. [1](#), [2](#), [7](#)
- [21] Rasheed A., Wahab, A., "Numerical analysis of an isotropic phase-field model with magnetic-field effect", *C.R. Acad. Sci. Paris, Ser. I*, Vol. **353**, pp. 219-224, 2015. [2](#)
- [22] Rasheed A., Belmiloudi A., "Phase-field method for computationally efficient modeling of the solidification of binary alloy with magnetic field effect", In. Proceedings of the NumAn2010 Conference in Numerical Analysis; Recent Approaches to Numerical Analysis: Theory, Methods and Applications, (eds., V. Dougalis, E. Gallopoulos, A. Hadjidimos et al.), pp. 222-230, 2010. [1](#)
- [23] Roplekar J. K., Dantzig J. A., "A study of solidification with a rotating magnetic field", *Int. J. Cast Met. Res.* Vol. **14**, pp. 79-95, 2001. [1](#)
- [24] Prescott P. J., Incropera F. P., "Magnetically damped convection during solidification of a binary metal alloy", *Trans. ASME*, Vol. **115**, pp. 302-310, 1993. [1](#)
- [25] Sampath R., "The adjoint method for the design of directional binary alloy solidification processes in the presence of a strong magnetic field", Thesis, Cornell University USA, 2001. [1](#)
- [26] Süli E., "Convergence and non-linear stability of Lagrange-Galerkin method for the Navier-Stokes equations.", *Numer. Math*, Vol. **53**, pp. 459-483, 1988. [4](#), [7](#)
- [27] Takaki T., Fukuoka T., Tomita Y., "Phase-field Simulations during Directional Solidification of a Binary Alloy using Adaptive Finite Element Method", *J. Crystal Growth*, Vol. **283**, pp. 263-278, 2005. [1](#)
- [28] Temam,R., "NavierStokes Equations", North-Holland, Amsterdam, 1977. [3](#)
- [29] Tonhardt R., Amberg G., "Simulation of natural convection effects on succinonitrile crystals", *Physical Review E*, Vol. **62**, No. 1, pp. 828-836, 2000. [1](#)
- [30] Tong X., Beckermann C., Kerma A., Li Q., "Phase-field simulations of dendritic crystal growth in a forced flow", *Physical Review E*, Vol **63**, pp. (061601-1)-(061601-16), 2001. [1](#)

- [31] Warren J. A., Boettinger W. J., “Prediction of dendritic growth and microsegregation patterns in a binary alloy using the phase-field method”, *Acta metall. mater*, Vol. 43, No. 2, pp. 689-703, 1995. [1](#), [2](#), [7](#)
- [32] Watanabe M., Vizman D., Friedrich J., Mueller G., “Large modification of crystal-melt interface shape during Si crystal growth by using electromagnetic Czochralski method”, *J. Crystal Growth*, Vol. **292**, pp. 252-256, 2006. [1](#)